RESEARCH ARTICLE | MARCH 07 2024

Improved operational unit process performance through three-dimensional design modifications using computational fluid dynamics method

Yazid Bindar ✉; Soen Steven; Pandit Hernowo; Pasymi Pasymi; Elvi Restiawaty

AIP Conf. Proc. 3073, 080003 (2024)
https://doi.org/10.1063/5.0199444

Improved Operational Unit Process Performance Through Three-Dimensional Design Modifications Using Computational Fluid Dynamics Method

Yazid Bindar[1, 2, 3, a)], Soen Steven[1, 3, b)], Pandit Hernowo[4, c)], Pasymi Pasymi[5, d)], and Elvi Restiawaty[1, 2, e)]

[1]*Department of Chemical Engineering, Faculty of Industrial Technology, Institut Teknologi Bandung, Bandung 40132, Indonesia*
[2]*Department of Bioenergy Engineering and Chemurgy, Faculty of Industrial Technology, Institut Teknologi Bandung, Sumedang 45363, Indonesia*
[3]*Biomass Technology Workshop, Faculty of Industrial Technology, Institut Teknologi Bandung, Sumedang 45363, Indonesia*
[4]*Department of Chemical Engineering, Institut Sains dan Teknologi Al-Kamal, Jakarta Barat 11520, Indonesia*
[5] *Department of Chemical Engineering, Faculty of Industrial Technology, Bung Hatta University, Padang, Indonesia*

[a)]*Corresponding author: ybybyb@itb.ac.id;*
[b)]*33019004@mahasiswa.itb.ac.id / soensteven201194@gmail.com;*
[c)]*pan_hernowo@ista.ac.id;*
[d)]*pasymi@bunghatta.ac.id;*
[e)]*elviwibisono@gmail.com*

Abstract. The designed process performances should be fulfilled by the selected proven technology. It has a set of allowable gaps which become the criteria for mechanical and process guarantees. They are quantified by temperature, pressure, yield or conversion, product purity, selectivity, mass flow, and flow behaviors. On the other hand, the designed performances are commonly obtained from long-time experiences in the process of technological development. In addition, gaps between designed and operational unit process performances should meet the acceptability criteria. Geometry is one factor that affects them. Nevertheless, the designed performances may not yet consider the detailed geometries for the operational performances. Another factor is the simplification in the designed stage which does not fit the actual process conditions. Therefore, this study intends to disclose the improvement of unit process performance using the computational fluid dynamics (CFD) method by including detailed geometries and actual conditions. The examined performances of unit processes were focused on three actual industrial cases: furnace, sand settling vessel, and boiler burner. Based on the results, improving the operational unit process performance using the CFD method is more attractive, accurate, and comprehensive.

INTRODUCTION

A technology regarding its performance is quantified and attributed by reliable and proven technology. The specified performances should be achieved when this technology is manufactured, constructed, and operated. They are determined in the process design. When the achieved performances in operation do not correspond to the performances of the design, the performance gaps exist which are symbolized by $\Delta\Phi_{OD}$. They cause problems from mild to severe levels. The development of technology should achieve these gaps as least as possible and even zero. For the specific performance parameters, such as the processing capacity that can be handled by the technology, the operating performance can be better than the design performance. This condition gives a positive difference. The performance gap values can also be negative or zero. Combinations of element performances generate the

International Seminar on Chemical Engineering Soehadi Reksowardojo (STKSR) 2022
AIP Conf. Proc. 3073, 080003-1–080003-14; https://doi.org/10.1063/5.0199444
Published by AIP Publishing. 978-0-7354-4872-8/$30.00

performances of technology. Even things that are considered trivial can cause the overall performance of the technology to be impaired.

The complexity of a developed technology depends on the number of technical elements. The elements can be grouped into mechanical (moving bodies), process conversion, structure material, energy, space, sensor, and control instrument elements. Each of these elements interacts with others. The more elements involved, the more complex technology is. The more complex the technology, the more unwanted performance gaps will dominate. A technology that has been commercialized gives the sense that the performance gaps of this technology have been known exactly by the developer who has designed, built, and operated this technology with the commercial specifications.

Unfortunately, improving operational unit process performance through three-dimensional design modifications using the computational fluid dynamics (CFD) method is a rarely discussed topic. A report by Zero Carbon Hub was concerned about closing the gap between design and as-built performance in terms of energy or carbon emission aspects [1]. Another publication by Donati and Paludetto (1997) reviewed the scale-up of chemical reactors from the small-scale experiment to achieve better performances with the help of mathematical models [2]. Still, the retrofit idea for a biodiesel production plant can be formulated using the thermodynamic process software ASPEN PLUS by comparing the performances of the existing and the modified plant [3]. Meanwhile, Ghawi and Kris (2011) improved the performance of a secondary clarifier in a wastewater plant treatment by modifying the inlet baffles using the CFD method [4]. The effect of various tray types in the distillation column was also reviewed by Patil and Patil (2016) for the operational and economic performances using a comparison method within the available performance data [5].

Embodying and obtaining opportunities in the design, construction, and operation stages for a commercial-scale technology are crucial steps for a technology developer. Thus, all the involved elements have their gap performances to be known. Engineering and financing problems become a serious barrier for the developer. These stages will produce detailed, comprehensive, actual, and accurate performance gap information. If these stages have not been realized, then the commercialization of the technology poses many risks. Based on the aforementioned exposition, exemplifies the CFD method for closing the gaps between operation and design in order to improve the actual industrial process performance is attractive and has its own novelty. The communicated scope is three actual industrial cases where their performances need to be improved, i.e. walking beam reheating furnace, sand settling vessel, and burner design for boiler purposes. Furthermore, it should be noted that this simulation involves detailed geometries and real process conditions.

GAPS IN UNIT PROCESS PERFORMANCES

A chemical plant is comprised of many unit processes [6,7]. Their performance has resulted from each unit process with the interdependent factors between connected unit processes. The analysis of the gap performances of the plant $\Delta\Phi_{OD,L}$ between the operation and the design become more complex. The gap performances for a unit process are indicated by $\Delta\Phi_{OD,i}$. The dependence of the gap performances for the whole plant with N number unit processes to each unit process can be generally stated as functions of:

$$\Delta\Phi_{OD,L} = f\left(\Delta\Phi_{OD,1}, \Delta\Phi_{OD,2}, \Delta\Phi_{OD3}, \dots, \Delta\Phi_{OD,N}\right) \quad (1)$$

The focus here is directed on the gap performances for a unit process in a chemical plant. Each unit process does a specific task of the process. A distillation column has the task of separating certain chemical components from the feed by the principles of relative volatility [3,8]. Combustor, gasifier, and pyrolyzer are unit processes for heating up the materials with the heat that is released by the fuel or biofuel combustion [9–17]. A boiler is used to generate high-pressure and high-temperature steam from the fuel combustion heat in the combustion chamber in efficient and safe conditions [18–25]. A chemical reactor and bioreactor should convert the feed to other products and chemicals at high rate, high conversion, selective, and as safe as possible [26–28]. A mixing or extraction equipment should also mix the materials well and uniformly at the outlet concentration and not spend energy [29–34].

A specific example of quantifying the performances of a unit process is a packed column distillation to separate ethanol from water in the ethanol solution. The capacity performances are the feed mass flow rate m_F, the vapor phase mass flow rate m_v, the liquid phase mass flow rate m_L, the top column mass flow rate m_T, and the bottom column mass flow rate m_B. The other two process performances are temperature T and pressure P in the column. The next performances are ethanol and water concentration C_i. The space performance of the column is identified by the diameter D and the height H. The flow dynamic performances inside the column are quantified by the liquid velocities $\overrightarrow{u_l}$ and the vapor velocities $\overrightarrow{u_g}$ within the column space. The height of the column is designed to facilitate the column to achieve the ethanol concentration on the top of the column. The column and the packing material performance are

quantified by M_C and M_P. This relates to the relative volatility (α), which is the ratio between the concentration ratio of ethanol to water in the vapor phase and liquid phase.

With the existence of the phase equilibrium along the column high with different T and P, the distillation undergoes a multistage phase equilibrium [8,35]. The theoretical stage number of the equilibrium in the column is identified as N_{TS}. The theoretical knowledge confirms that the higher the purity of the ethanol on the top column, the higher the N_{TS}. The packed column is packed with packing material shapes β_S to make an effective contact between vapor and liquid phases in the column. Various shapes of packing have been developed as the technological improvement that was based on the operational experiences of this distillation column technology [36]. The packing shapes generate the pressure drop ΔP performance along the column. The packing types also are correlated to the flooding performance F. The reflux performance on the top column is identified by the reflux ratio R_R. The liquid level performance on the bottom of the column is stated by L_l. The reboiler performances are represented by R_B. The condenser performances are said to be R_C. The reflux pump performances are stated by R_P. Therefore, the performance parameters for a packed distillation column are represented by Φ_{PD} which is written as Eq. (2). These parameters are then a lumped parameter Φ_{SB}, the designed performances for a unit process are stated by Φ_{Di}, and the operational performances for this unit are obtained as Φ_{Oi}. The gaps in the unit process performances are then defined by Eq. (3). These gaps $\Delta\Phi_{OD,i}$ have to be acquired. By knowing these gaps, the technology of that unit process can be pursued to go to the commercial stage with guaranteed specifications without a doubt. Nine stages in the technology development of the unit process start from the research idea formulation and arrive at the commercialization stage, Figure 1.

$$\Phi_{PD} \equiv \begin{bmatrix} m_F, m_v, m_L, m_T, m_B, T, \\ P, C_i, D, H, \overrightarrow{u_l}, \overrightarrow{u_g}, \alpha, \\ N_{TS}, \beta_S, M_C, M_P, \Delta P, F, \\ R_R, L_l, R_B, R_C, R_P \end{bmatrix} \tag{2}$$

$$\Delta\Phi_{OD,i} = \Phi_{Oi} - \Phi_{Di} \tag{3}$$

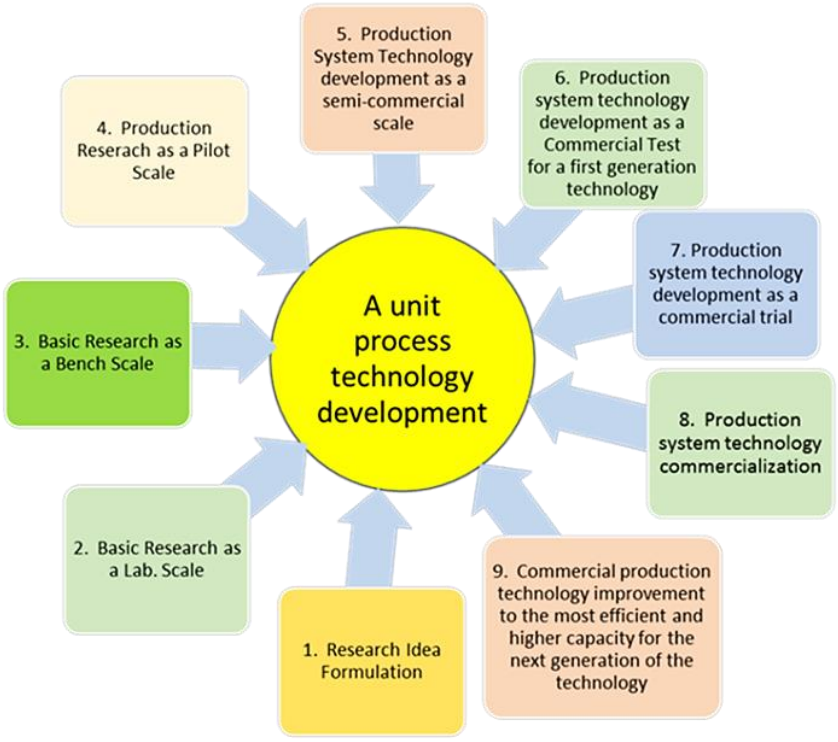

FIGURE 1. Nine stages of a unit process technology development.

The proven or mature technology reaches the stage of technology commercialization. At this stage, the designed specifications will be achieved without any risk to operational performance. When the semi-commercial stage is still developing and the technology development is forced to jump to the commercial stage, then the gaps between the operational commercial performances and the designed ones will be negatively wider. It can be postulated that the

gaps $\Delta\Phi_{OD,i}$ from stages 1-9 will be getting closer. The time duration t_{TD} to the arrival on the commercial stage should be as shorter as possible. The cost of the development C_{TD} should be minimized. These three parameters are hypothetically correlated to the stages of technology development as shown in Figure 2.

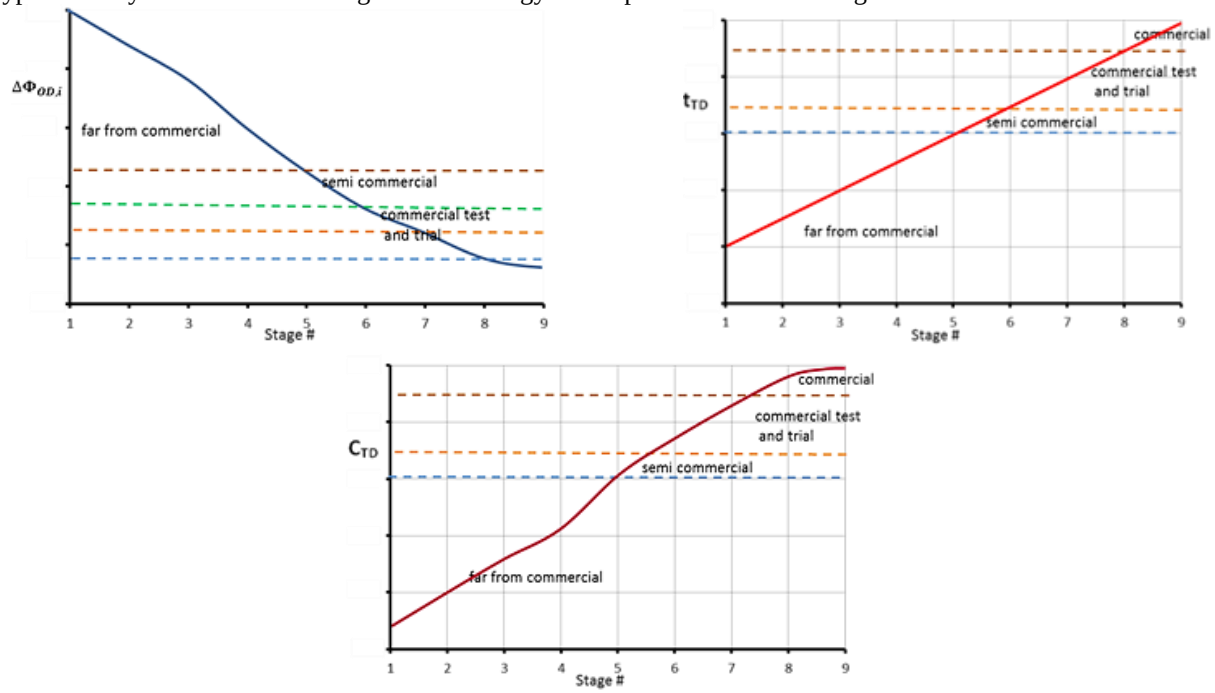

FIGURE 2. Characteristics of gaps, time duration, and cost in technology development.

The most important thing in technology development is to establish the previous nine stages to be done. Nevertheless, several constraints exist, such as the lack and shortage of motivation, the unstructured objectives and programs, fewer human resource competencies and professional skills, less financial capability, poor linkage and support between university-industry-government, and stronger competitors for the similar technology being developed [37]. These constraints should be handled with various strategies. The closer gaps in the technology performances $\Delta\Phi_{OD,i}$, the shorter development time t_{TD} and the minimum development cost become the objective functions in the technology development. The real gaps can be acquired if the full-scale commercial technology is designed, constructed, and operated [38–40]. However, this stage is not easy to be delivered, and the opportunity is sometimes not available.

For the objective of closing the gaps between the design and the operational performances, the design methodology is improved at present with a full mathematical modeling method that is derived from the detailed phenomena that govern the unit process behaviors. The unit process behaviors are then predicted comprehensively within the three-dimensional space coordinates and the operating time. The process performances of a unit process are quantified by temperature T, mass fraction of the chemical components ω_j, pressure P, and velocity components u_x, u_y, and u_z. All these variables abide by the conservation equations that govern the process phenomena. These are generally expressed in Eq. (4), while the performance gaps between the operated and the designed process for the above performance variables are defined by Eq. (5).

$$T = f_1(x,y,z,t)\ ;\ \omega_j = f_2(x,y,z,t)\ ;\ P = f_3(x,y,z,t)\ ; \tag{4}$$
$$u_x = f_4(x,y,z,t)\ ;\ u_y = f_5(x,y,z,t)\ ;\ u_z = f_6(x,y,z,t)$$

$$\Delta T_{OD,i} = T_{Oi} - T_{Di}\ ;\ \Delta\omega_{j_{OD,i}} = \omega_{j_{Oi}} - \omega_{j_{Di}}\ ;\ \Delta P_{OD,i} = P_{Oi} - P_{Di}\ ; \tag{5}$$
$$\Delta u_{x_{OD,i}} = u_{x_{Oi}} - u_{x_{Di}}\ ;\ \Delta u_{y_{OD,i}} = u_{y_{Oi}} - u_{y_{Di}}\ ;\ \Delta u_{z_{OD,i}} = u_{z_{Oi}} - u_{z_{Di}}$$

CFD METHOD

The conventional method of process technology development is done by following the stepwise procedure in Figure 1. Each step in this conventional method employs simplified and empirical mathematical model equations for

representing the transport phenomena. The design procedures are derived from these simple process models. The pilot-scale is continued to scale up the process by increasing the size and the capacity of the unit process being developed. The cycle of development in the conventional method is described by the blue line cycle in Figure 3. The more advanced method in obtaining the designed performances of the being developed technology employs three-dimensional and time-dependent governing equation models. These mathematical equation models transform the actual process to the modeled ones with the involvement of the actual shape and size with the three-dimensional geometry of the unit process, as given in Figure 4. The equation models are solved numerically as advanced computational methods with the support of computers.

The comprehensive and advanced computational process design procedures take over the conventional design procedures. The cycle of the advanced process design procedures is shown by the red line cycle in Figure 3. These computing methods for transport phenomena equations are lumped into a single computing engine. Many things are beneficial to the development of process technology using this technique with the red line cycle in Figure 3. The traditional path requires a long time of industrial experience. These long-time experiences can be shortened by the involvement of the CFD, and the various innovations can be explored at a lower cost by the development [41,42].

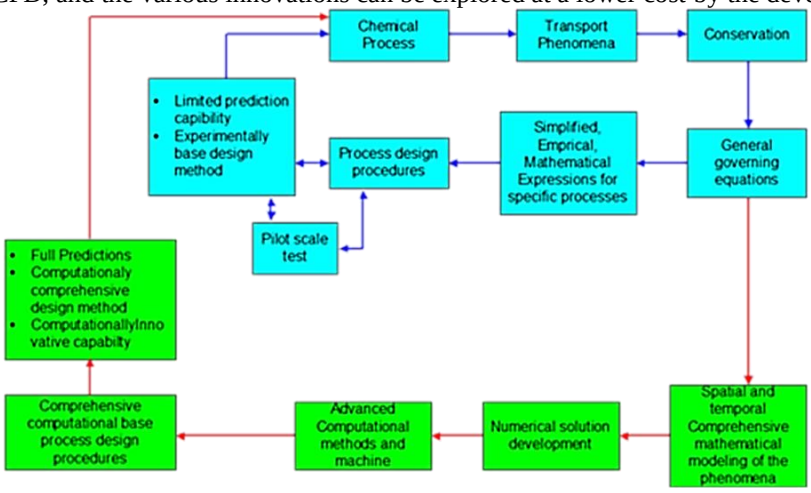

FIGURE 3. Advanced process design procedures using the CFD method for unit processes technology development.

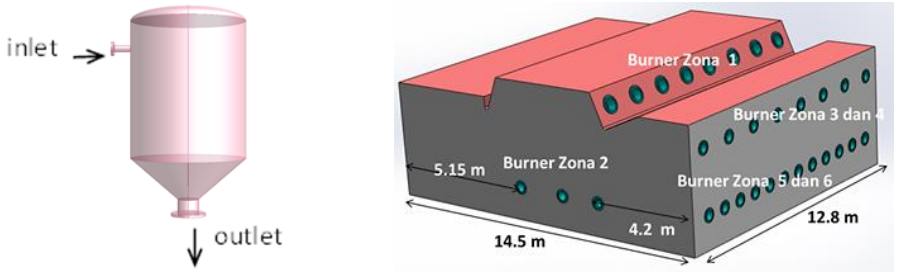

FIGURE 4. Actual shape and size of unit processes.

The basic equations that govern the process are described by the fluid flow governing equations that are characterized by the turbulent flow phenomena [43–47]. The variable performances of the turbulent flow are velocity components ($\bar{u}_x$, $\bar{u}_y$, and $\bar{u}_z$), static pressure p, turbulent kinetic energy k, turbulent energy dissipation rate ε, and turbulent viscosity μ_t. The physical properties are density ρ and laminar viscosity μ. Gravitational constants are g_x, g_y, and g_z. The turbulent quantities are generated by the fluctuation velocity components (u_x', u_y', and u_z'). The conservation model equations are formulated as in Eqs (6)-(13) [48–53].

$$\frac{\partial \rho}{\partial t} + \frac{\partial (\overline{\rho u_x})}{\partial x} + \frac{\partial (\overline{\rho u_y})}{\partial y} + \frac{\partial (\overline{\rho u_z})}{\partial z} = 0 \tag{6}$$

$$\rho \frac{\partial \bar{u}_x}{\partial t} + \rho \bar{u}_x \frac{\partial \bar{u}_x}{\partial x} + \rho \bar{u}_y \frac{\partial \bar{u}_x}{\partial y} + \rho \bar{u}_z \frac{\partial \bar{u}_x}{\partial z} = -\frac{\partial \bar{p}}{\partial x} + \frac{\partial}{\partial x}\left[(\mu + \mu_t)\frac{\partial \bar{u}_x}{\partial x}\right] + \frac{\partial}{\partial y}\left[(\mu + \mu_t)\frac{\partial \bar{u}_x}{\partial y}\right] + \frac{\partial}{\partial z}\left[(\mu + \mu_t)\frac{\partial \bar{u}_x}{\partial z}\right] + \rho g_x \tag{7}$$

$$\rho\frac{\partial\bar{u}_y}{\partial t}+\rho\bar{u}_x\frac{\partial\bar{u}_y}{\partial x}+\rho\bar{u}_y\frac{\partial\bar{u}_y}{\partial y}+\rho\bar{u}_z\frac{\partial\bar{u}_y}{\partial z}=-\frac{\partial\bar{p}}{\partial y}+\frac{\partial}{\partial x}\left[(\mu+\mu_t)\frac{\partial\bar{u}_y}{\partial x}\right]+\frac{\partial}{\partial y}\left[(\mu+\mu_t)\frac{\partial\bar{u}_y}{\partial y}\right]+\frac{\partial}{\partial z}\left[(\mu+\mu_t)\frac{\partial\bar{u}_y}{\partial z}\right]+\rho g_z \quad (8)$$

$$\rho\frac{\partial\bar{u}_y}{\partial t}+\rho\bar{u}_x\frac{\partial\bar{u}_y}{\partial x}+\rho\bar{u}_y\frac{\partial\bar{u}_y}{\partial y}+\rho\bar{u}_z\frac{\partial\bar{u}_y}{\partial z}=-\frac{\partial\bar{p}}{\partial y}+\frac{\partial}{\partial x}\left[(\mu+\mu_t)\frac{\partial\bar{u}_y}{\partial x}\right]+\frac{\partial}{\partial y}\left[(\mu+\mu_t)\frac{\partial\bar{u}_y}{\partial y}\right]+\frac{\partial}{\partial z}\left[(\mu+\mu_t)\frac{\partial\bar{u}_y}{\partial z}\right]+\rho g_z \quad (9)$$

$$\rho\frac{\partial k}{\partial t}+\rho\bar{u}_x\frac{\partial k}{\partial x}+\rho\bar{u}_y\frac{\partial k}{\partial y}+\rho\bar{u}_z\frac{\partial k}{\partial z}=\frac{\partial}{\partial x}\left[\left(\mu+\frac{\mu_t}{\sigma_k}\right)\frac{\partial k}{\partial x}\right]+\frac{\partial}{\partial y}\left[\left(\mu+\frac{\mu_t}{\sigma_k}\right)\frac{\partial k}{\partial y}\right]+\frac{\partial}{\partial z}\left[\left(\mu+\frac{\mu_t}{\sigma_k}\right)\frac{\partial k}{\partial z}\right]+G_k-\rho\varepsilon \quad (10)$$

$$\rho\frac{\partial\varepsilon}{\partial t}+\rho\bar{u}_x\frac{\partial\varepsilon}{\partial x}+\rho\bar{u}_y\frac{\partial\varepsilon}{\partial y}+\rho\bar{u}_z\frac{\partial\varepsilon}{\partial z}=\left[\left(\mu+\frac{\mu_t}{\sigma_\varepsilon}\right)\frac{\partial\varepsilon}{\partial x}\right]+\frac{\partial}{\partial y}\left[\left(\mu+\frac{\mu_t}{\sigma_\varepsilon}\right)\frac{\partial\varepsilon}{\partial y}\right]+\frac{\partial}{\partial z}\left[\left(\mu+\frac{\mu_t}{\sigma_\varepsilon}\right)\frac{\partial\varepsilon}{\partial z}\right]+C_{\varepsilon1}\frac{\varepsilon}{k}G_k-C_{\varepsilon2}\rho\frac{\varepsilon^2}{k} \quad (11)$$

$$\mu_t=C_\mu\rho\,k^2/\varepsilon \quad (12)$$

$$G_k=2\mu_t\left[\left(\frac{\partial\bar{u}_x}{\partial x}\right)^2+\left(\frac{\partial\bar{u}_y}{\partial y}\right)^2+\left(\frac{\partial\bar{u}_z}{\partial z}\right)^2\right]+\mu_t\left(\frac{\partial\bar{u}_x}{\partial y}+\frac{\partial\bar{u}_y}{\partial x}\right)^2+\mu_t\left(\frac{\partial\bar{u}_x}{\partial z}+\frac{\partial\bar{u}_z}{\partial x}\right)^2+\mu_t\left(\frac{\partial\bar{u}_z}{\partial y}+\frac{\partial\bar{u}_y}{\partial z}\right)^2 \quad (13)$$

The constants are $c_\mu=0.09$, $\sigma_k=1.0$, $\sigma_\varepsilon=1.3$, $c_{\varepsilon1}=1.44$, and $c_{\varepsilon2}=$ 1,92.

A unit process may involve chemical conversions with the rate of the chemical reaction $\bar{R}_j$ for a chemical component j. This process may also be followed by the thermal energy transfer with the variable T. The chemical species transport equations with the variable of mass fraction of a chemical species $\overline{\omega_j}$ are added to the above equations as in Eq. (14). The additional transport property is the binary molecular diffusivity D_j of the species j. $N_{Sc,t}$ is the turbulent Schmidt number. The energy thermal transfer equation for the temperature performance T is formulated in Eq. (15). The generated rate of the heat from the N chemical reactions is obtained as $\sum_j^N \bar{R}_j\,\Delta h_{rj}$. The involved molecular thermal properties are specific heat capacity c_p and thermal conductivity λ. The contribution of the turbulent flow to the thermal conductivity is stated as the turbulent thermal conductivity λ_t. The turbulent thermal conductivity is evaluated from Eq. (16). The turbulent Prantl number $N_{pr,t}$ is estimated at 0.85. S_T is the rate of the heat source that comes and leaves to and from the volume due to radiation.

$$\rho\frac{\partial\overline{\omega_j}}{\partial t}+\bar{u}_x\frac{\partial\overline{\omega_j}}{\partial x}+\bar{u}_y\frac{\partial\overline{\omega_j}}{\partial y}+\bar{u}_z\frac{\partial\overline{\omega_j}}{\partial z}=\frac{\partial}{\partial x}\left[\left(\rho D_i+\frac{\mu_t}{\rho N_{Sc,t}}\right)\frac{\partial\overline{\omega_j}}{\partial x}\right]+\frac{\partial}{\partial y}\left[\left(\rho D_j+\frac{\mu_t}{\rho N_{Sc,t}}\right)\frac{\partial\overline{\omega_j}}{\partial y}\right]+\frac{\partial}{\partial z}\left[\left(\rho D_j+\frac{\mu_t}{\rho N_{Sc,t}}\right)\frac{\partial\overline{\omega_j}}{\partial z}\right]+\rho M_j\bar{R}_j+S_{\omega_j} \quad (14)$$

$$\frac{\partial(\rho c_p\bar{T})}{\partial t}+\overline{u_x}\frac{\partial(\rho c_p\bar{T})}{\partial x}+\overline{u_y}\frac{\partial(\rho c_p\bar{T})}{\partial y}+\overline{u_z}\frac{\partial(\rho c_p\bar{T})}{\partial z}=\frac{\partial}{\partial x}\left[(\lambda+\lambda_t)\frac{\partial\bar{T}}{\partial x}\right]+\frac{\partial}{\partial y}\left[(\lambda+\lambda_t)\frac{\partial\bar{T}}{\partial y}\right]+\frac{\partial}{\partial z}\left[(\lambda+\lambda_t)\frac{\partial\bar{T}}{\partial z}\right]+\sum_j^N\bar{R}_j\,\Delta h_{rj}+S_T \quad (15)$$

$$\lambda_t=\frac{c_p\mu_t}{N_{pr,t}} \quad (16)$$

The above equations for the performance variables $\bar{u}_x$, $\bar{u}_y$, $\bar{u}_z$, $\bar{p}$, k, ε, $\bar{T}$ and $\overline{\omega_j}$ are solved numerically using CFD. The procedures are well formulated, developed, and described by Patankar (1980) [54] and Chung (2010) [55]. The actual scale geometry, shape, and arrangement of the unit process are computationally constructed to replace the physical unit process before it is erected as the real physics unit at the actual field site. Therefore, the gaps to occur between the operational and designed performances are well predicted and the confidence to obtain the operational performances being closer to the designed performances is high.

The simulation for all cases in this study was in steady-state mode and under tetrahedral grid with a total number of 2,000,000 as it had already been independent of grid number alteration. The algorithm for solving all cases was coupled method which required spatial discretization methods consisting of least square cell scheme for gradient and QUICK scheme for pressure, momentum, pressure, turbulent kinetic energy, turbulent kinetic dissipation rate, energy, and species component. The relaxation factors for numerical calculation were set at 0.5 for pressure, 0.5 for momentum, 0.25 for density, 1 for body forces, 0.75 for turbulent kinetic energy, 0.75 for turbulent kinetic dissipation rate, 1 for turbulent viscosity, 0.75 for species components, and 0.75 for energy. Also, the calculation was set at 2000 iterations until convergent and the difference reached 10^{-6}.

RESULTS AND DISCUSSION

Industrial Case 1: Walking Beam Reheating Furnace Improvement

The apparatus was designed with a capacity of 70 tonnes/h and dimensions of 14.5 m in length, 12.8 m in width, and 8 m in height (Figure 5). The furnace utilized natural gas as fuel which consisted of 88.6% CH_4, 5.8% hydrocarbon gases, and 5.6% CO_2. The heating value of the fuel was 8650 kcal/Nm^3. Fuel was injected at flow rates of 50-60 Nm^3/h while the combustion air was fed at 9-10 times of flow rates. The problem found was the attendance of hotspots at several locations in burners which consequently declined their thermal efficiency. It was caused by the not suitable design of the reheating furnace for the heating process. It was also found that the current temperature of burner zones was much higher than the designed temperature which was reflected by more than 50% of the generated heat was not absorbed by billets under the operational firing rate.

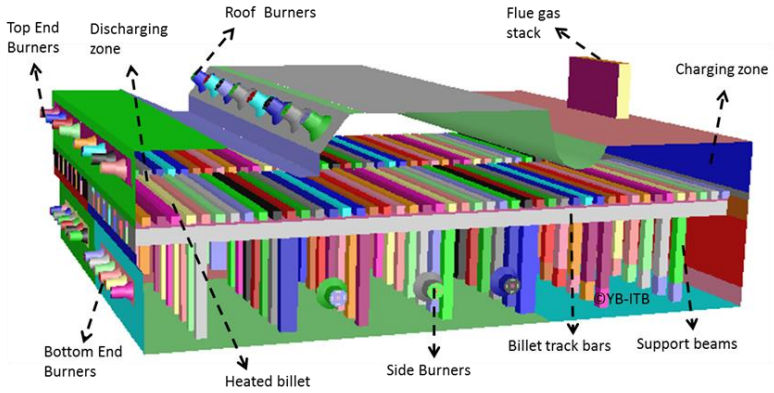

FIGURE 5. Walking beam reheating furnace.

The performance of burners and furnaces was then evaluated to optimize the heat distribution and thermal efficiency in the reheating furnace in order to economize fuel consumption. Besides, the quality of combustion for each burner should be noted, particularly in the use of excess air and the fuel mixing performance between fuel and combustion air to achieve the desired temperature [56]. According to field experiences, several proposed modifications to solve the problem were relocating burner locations, reducing furnace volume, and reformulating burner and furnace setting parameters. Those modifications were done to obtain the maximum thermal efficiency for fuel-saving.

The first modification was by relocating two side burners from the downstream to the upstream position, Figure 6. Each side wall furnace had three burners. The downstream pair side burners were relocated from the original positions towards the upstream position. This was done to reduce the combustion gases not being sucked directly into the recuperator tower. It was expected to provide an opportunity for exchanging the heat between hot gas and billets. The next modification was followed by reducing some portions of the top and the bottom volumes and removing all the roof burners, Figure 7.

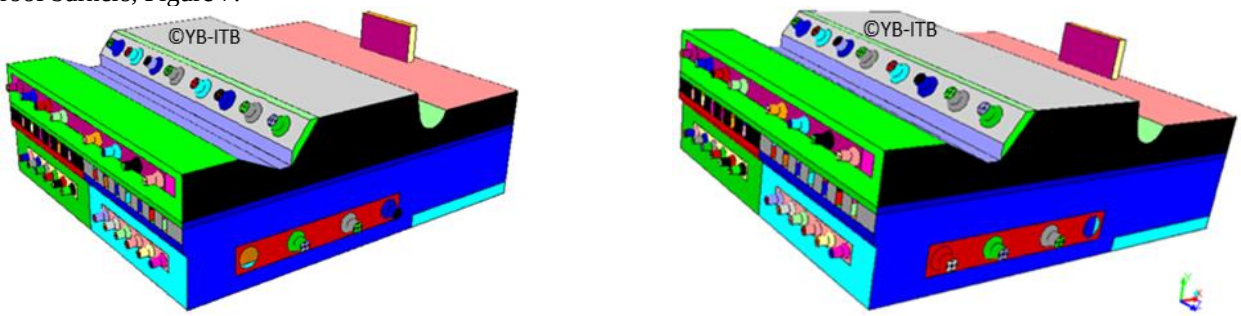

FIGURE 6. Walking beam furnace original design (left); Walking beam furnace modification by relocating side burners (right).

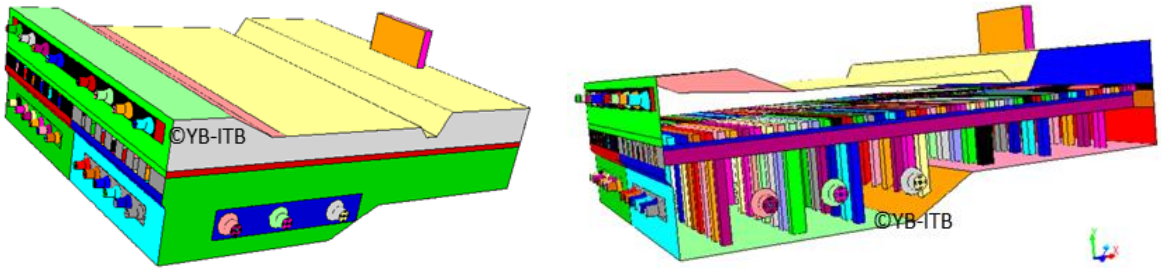

FIGURE 7. Walking beam furnace volume reduction without roof burners.

The CFD method revealed detailed information to examine the effects of relocations of these burners. The flow pathlines were chosen to characterize the flow behaviors inside both furnaces and did not show a significant change (Figure 8). Besides, hot gases from the burners were visualized closer to the downstream area whereas it was directly sucked by the recuperator as in Figure 9. The concern was a shifting pattern of the billet heating that was more intensively distributed towards the discharge area.

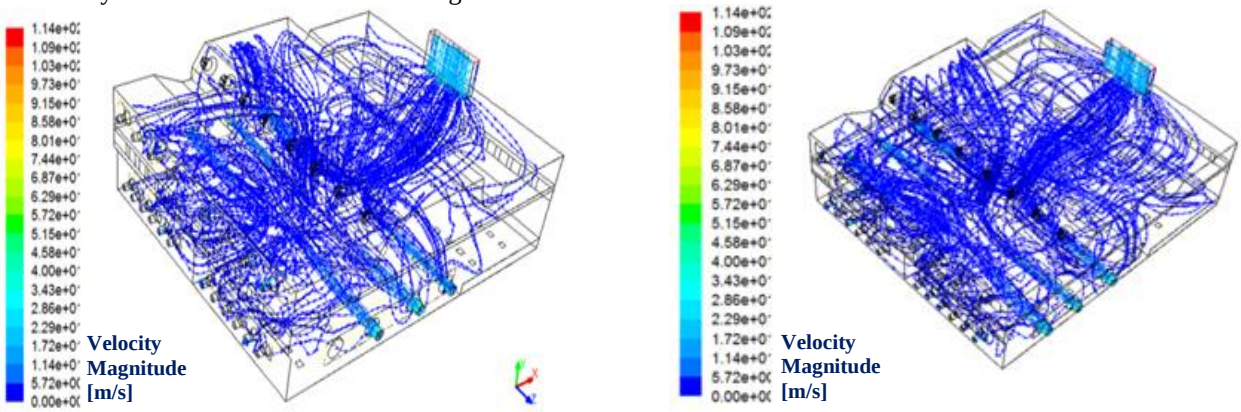

FIGURE 8. Flow pathlines of side burners inside the walking beam furnace for the original design (left) and the modification by the relocation of side burners (right).

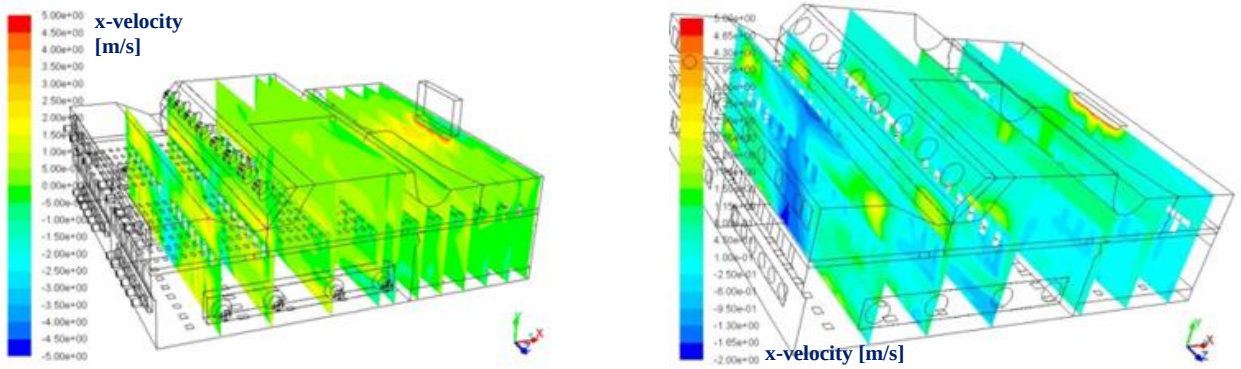

FIGURE 9. Contours of the x-velocity component at various planes inside the walking beam furnace for the original design (left) and the modification by the relocation of side burners (right).

On the other hand, the results for the flow simulation within the modified furnace by reducing some portions of the volume are comprehensively compared. These results point out that the portion of the gas flow rate of the combustion gas in the furnace bottom becomes dominant, Figure 10. According to Figure 11, up to the 11.15 m axial distance from the discharge door, the heating of the bottom furnace is more dominant. After this distance, the portions of the combustion gas at the bottom furnace are still larger than in the original conditions. The CFD results confirmed that modification by means of furnace volume reduction can produce a more stable heat inside the modified furnace. However, the bottom support beams still have a possibility to have higher temperatures.

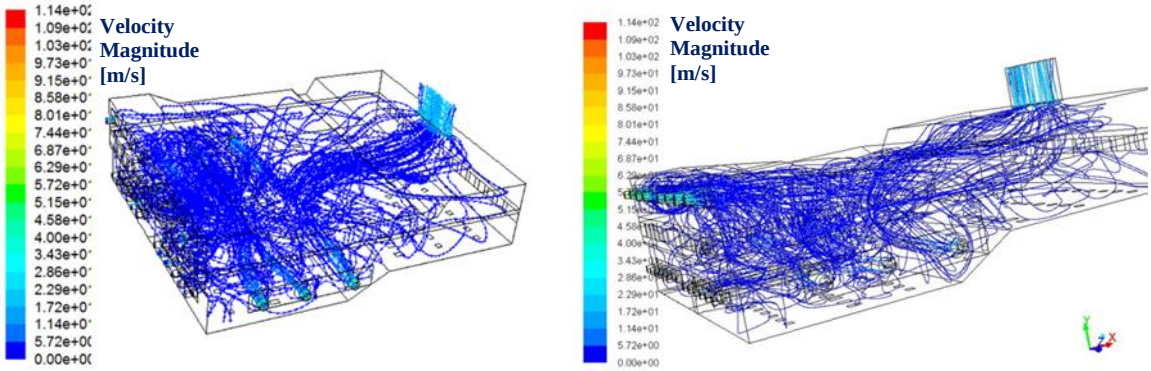

FIGURE 10. Flow pathlines with the releasing points from the side burners inside the walking beam furnace for the original design (left) and the modification by volume reduction without roof burners (right).

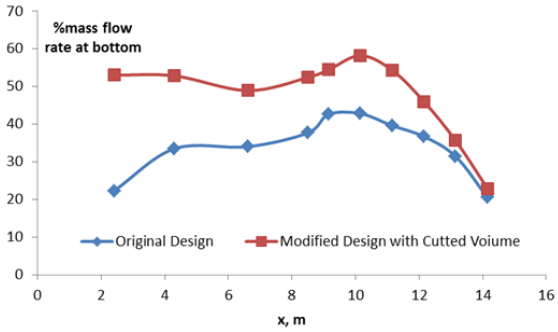

FIGURE 11. Mass flow rate percentage at the bottom furnace for the original design and the modification by volume reduction without roof burners.

Industrial Case 2: Sand Settling Vessel Design Analysis and Separation Improvement

The gas and oil surface facilities are usually equipped with sand removal units which are fed with incoming fluid feed prior to the oil-water-gas separation units [57]. The common problem for the sand separator is that the outlet liquids still contain fine sand. This problem is indicated by the presence of sand in the internal walls of the produced water mechanical equipment such as de-oiler, reject oil separator, and sump caisson [58,59]. The above phenomenon becomes a poor indication of the removal performance of the sand separator units. Therefore, this sand vessel problem should be solved.

The modification inside the vessel chamber was carried out by simulation and the transport models in the settling sand vessel involve Eqs. (6)-(13). The solid sand particle movements or trajectories together with the fluid inside the vessel were examined using the discrete phase model. The particle density is stated as ρ_p. The additional accelerations in x, y, and z directions due to additional working forces are a_x, a_y, and a_z. In addition, t_{Dx}, t_{Dy}, and t_{Dz} are the drag times due to the drag forces that are defined in Eqs. (19)-(20). The particle trajectories were quantified by the velocity components as $\bar{u}_{px}$, $\bar{u}_{py}$, and $\bar{u}_{pz}$. The force balance acting on the particle is written in Eq. (21) [45,60]. The drag coefficient C_D is a function of the Reynold number. A most common drag coefficient function is given by Morsi and Alexander (1972) as a polynomial function of the variable $1/N_{Re}$ [61]. The particle diameter is represented by d_p.

$$t_{Dx}=\frac{\rho_p d_p^2}{18\mu}\frac{24}{C_D N_{\mathrm{Re},x}}\quad;\quad t_{Dy}=\frac{\rho_p d_p^2}{18\mu}\frac{24}{C_D N_{\mathrm{Re},y}}\quad;\quad t_{Dz}=\frac{\rho_p d_p^2}{18\mu}\frac{24}{C_D N_{\mathrm{Re},z}} \tag{17}$$

$$N_{\mathrm{Re},x}=\frac{d_p\left|\bar{u}_x-\bar{u}_{px}\right|\rho}{\mu}\quad;\quad N_{\mathrm{Re},y}=\frac{d_p\left|\bar{u}_y-\bar{u}_{py}\right|\rho}{\mu}\quad;\quad N_{\mathrm{Re},z}=\frac{d_p\left|\bar{u}_z-\bar{u}_{pz}\right|\rho}{\mu} \tag{18}$$

$$\frac{\partial\bar{u}_{px}}{\partial t}=\frac{\left(\bar{u}_x-\bar{u}_{px}\right)}{t_{Dx}}+\frac{g_x\left(\rho_p-\rho\right)}{\rho_p}+a_x\quad;\quad \frac{\partial\bar{u}_{py}}{\partial t}=\frac{\left(\bar{u}_y-\bar{u}_{py}\right)}{t_{Dy}}+\frac{g_y\left(\rho_p-\rho\right)}{\rho_p}+a_y\quad;\quad \frac{\partial\bar{u}_{pz}}{\partial t}=\frac{\left(\bar{u}_z-\bar{u}_{pz}\right)}{t_{Dz}}+\frac{g_z\left(\rho_p-\rho\right)}{\rho_p}+a_z \tag{21}$$

Sand settling vessel had diameter of 90 in and height of 149 in, Figure 12. The operating conditions of this vessel were set with oil flow rate of 7.95 lbm/s, water flow rate of 119 lbm/s, and sand flow rate of 0.0147 lbm/s. The sand

particle diameters range from 20-100 µm with 0.8 of mass fraction and less than 20 µm with 0.2 of mass fraction. From the simulation, results confirmed that severe and intense flows occurred from the top to the bottom, Figure 13a. It happened due to the orientation of the inlet and the outlet pipe that is closer to each other. This leads to the ease of sand particles being entrained before complete separation. It was reinforced by the maximum particle residence time recorded at 71 s (Figure 13c). Thus, the original vessel design gave poor sand removal efficiency of only 2.2%.

Because the particle residence time inside the vessel was too swift, the modification should gave conditions that prolonged the particle trajectory [35]. Adding a vertical baffle inside the vessel was then proposed and conducted. After modification, the oil and water recirculation flows were captured (Figure 13b) and the sand residence time lengthened to 399 s (Figure 13d). Hence, the sand removal efficiency in the modified vessel design was rectified by up to 15%.

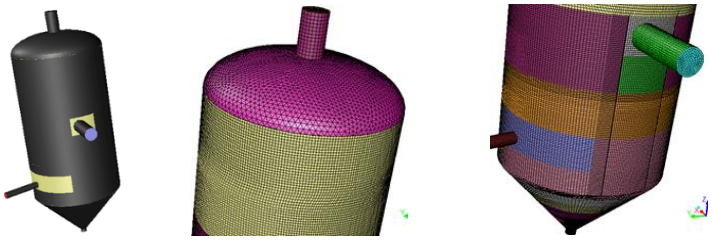

FIGURE 12. The geometry and the mesh form of a sand settling vessel.

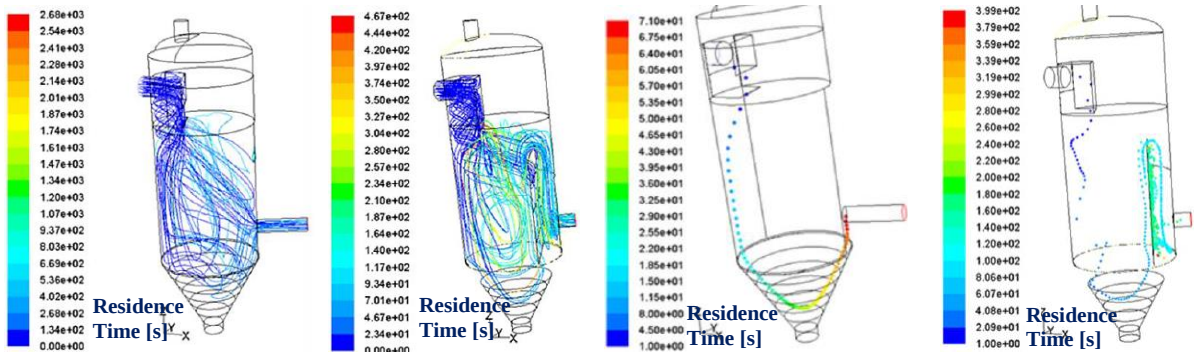

(a) (b) (c) (d)

FIGURE 13. The flow pathlines for the sand settling vessel before modification (a) and after modification by adding baffle (b); The single particle trajectory for the sand settling vessel before modification (c) and after modification by adding baffle (d).

Industrial Case 3: Boiler Burner Design Modification

For case 3, an industrial boiler unit has a capacity of 90 tonnes/h. According to the design conditions, steam specifications were 40 bar atm for pressure and 400°C for temperature. This boiler employed natural gas as a fuel. According to the energy audit evaluation, the boiler was only capable of operating at below 50 tonnes/h. Increasing the flow rates of natural gas also caused the steam temperature to rise and surpass the set temperature. The main problem was the inability to achieve rapid mixing between air and fuel in the area near the burner and in the boiler combustion chamber.

In consequence, this burner design required to be improved. The proposed solution was to modify the burner geometries through CFD method. The existing burner had gas fuel pipes, 9 fuel holes, perforated barrier plates, and round-shaped edges, whereas the modified one had sharp edges to intensify the air and fuel mixing area as shown in Figure 14. Also, the divergence angle of burner mouth was enhanced from 25° to 30° in order to stabilize the flame.

Natural gas for boiler fuel consisted of 92.7% CH_4, 4.2% C_2H_6, and the rest was CO_2. Combustion air used was composed of 79% N_2 and 21% O_2. The component concentration, temperature, and flow pathlines represented the performance variables. Before modification, the supply of air and fuel was not balanced (Figure 15a left), only a small fraction of fuel flew through the holes in the barrier plates (Figure 15b left), and the temperature distribution was not homogeneous due to an imbalance in air distribution (Figure 16 left).

After modification through CFD method, the balance amount of air and fuel supply can be realized (Figure 15a right), the fuel sprayed was evenly distributed through the holes in the barrier plates (Figure 15b right), the uniform temperature distribution at the location after the burner mouth was achieved (Figure 16 right), and the well and stable

mixing of fuel and air (Figure 17). It was indicated that modification by CFD method reveals a meaningful improvement in burner boiler performance.

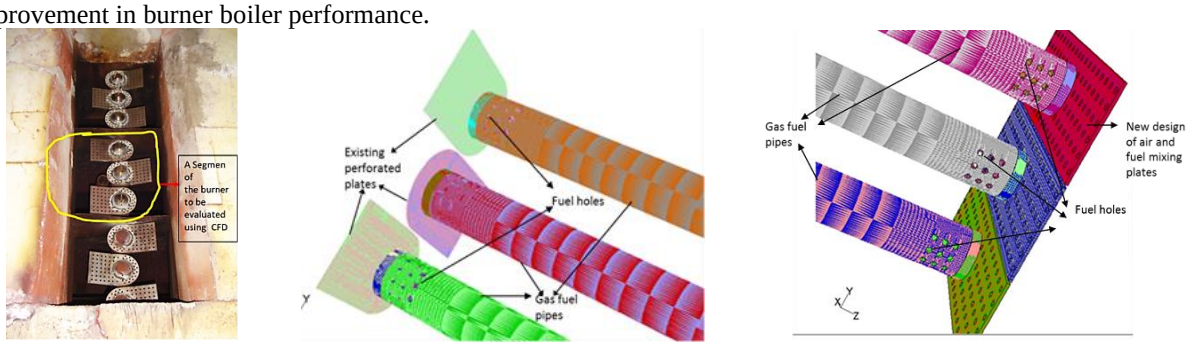

FIGURE 14. An existing multi-holes with 9 pipes (left and middle) and a modified gas burner (right).

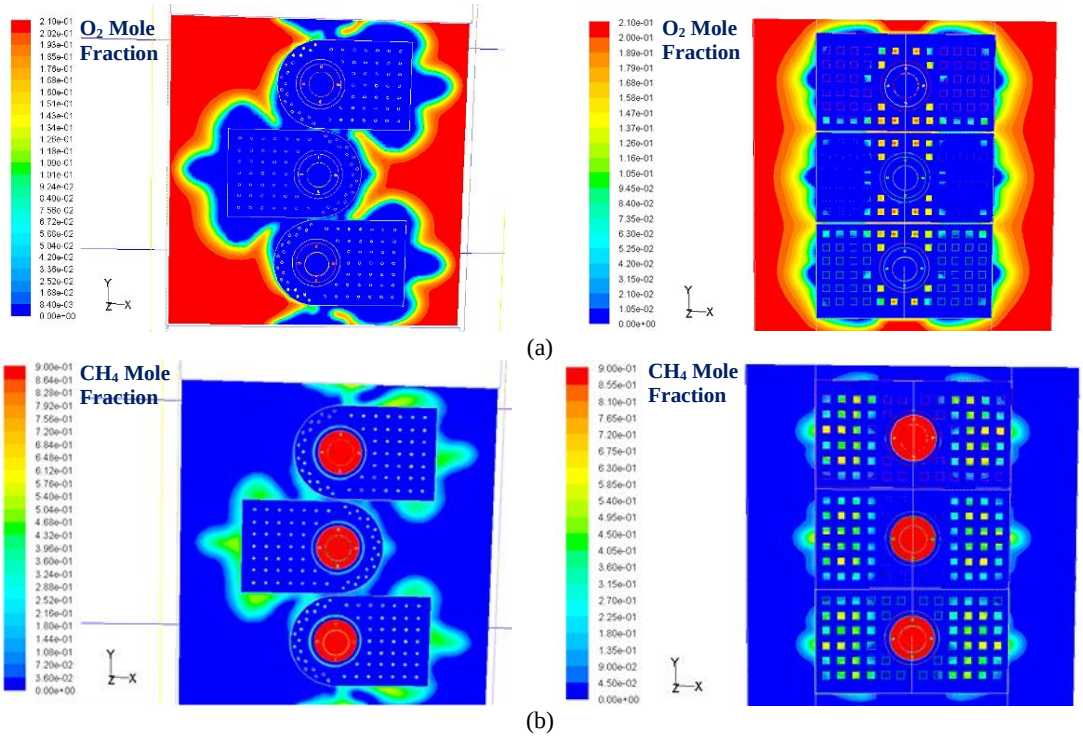

FIGURE 15. Concentration distribution on the mouth of existing burner (left) and modified (right) burner for oxygen (a) and methane (b)

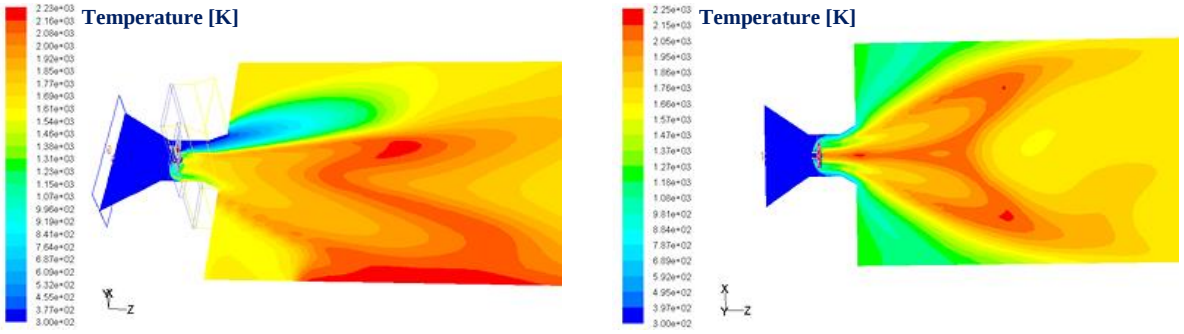

FIGURE 16. Temperature distribution of existing burner (left) and modified burner (right) in a middle y-plane.

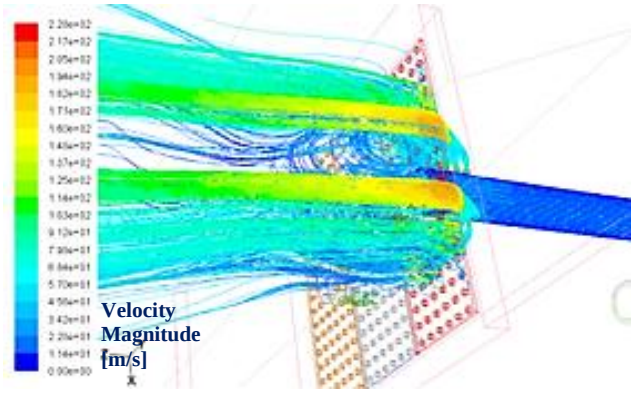

FIGURE 17. Air and methane pathlines on the stabilizing and mixing plates of the modified burner.

CONCLUSION

The performance gaps are proposed as the differences between the operational performances and the designed performances. They are aimed to quantify a proven technology of a process plant. The whole plant performances are built by performance gaps of each unit process involved. The cycle of technology development involves time, cost, and risks. These three burdens can be minimized using comprehensive knowledge and engineering tools in the design stage. The CFD method has been shown to fulfill it for predicting unit process performances. The process improvement of three unit processes in actual industrial cases (walking beam reheating furnace, sand settling vessel, and boiler burner) with various design parameters are exemplified to obtain all the performance variables such as temperature, flow pathlines, components concentration, pressure, and turbulent quantities. Improving the operational unit process performance gaps with CFD method are conclusively more attractive, accurate, and comprehensive.

REFERENCES

1. Zero Carbon Hub, *Closing the Gap Between Design and As-Built Performance: End of Term Report* (The Zero Carbon Hub, London, 2014).
2. G. Donati and R. Paludetto, Catal. Today **34**, 483–533 (1997).
3. N. Nguyen and Y. Demirel, Energy **35**, 1625–1632 (2010).
4. A. G. Ghawi and J. Kris, Slovak J. Civ. Eng. **19**, 1–11 (2011).
5. N. P. Patil and V. S. Patil, "Operational and Economic Assessment of Distillation Column from the Performance of Tray" in *International Conference on Global Trends in Engineering, Technology, and Management* (2016), pp. 500–505.
6. J. Haydary, *Chemical Process Design and Aspen Plus and Aspen HYSYS Applications*, 1st ed. (American Institute of Chemical Engineers, John Wiley & Sons, 2019).
7. K. I. M. Al-Malah, *ASPEN PLUS® Chemical Engineering Applications* (John Wiley & Sons, 2017).
8. J. D. Seader, E. J. Henley, and D. K. Roper, *Separation Process Principles: Chemical and Biochemical Operations, Third Edition* (John Wiley & Sons, Inc., 2011).
9. S. Steven, P. Hernowo, E. Restiawaty, A. Irawan, C. B. Rasrendra, A. Riza, and Y. Bindar, Waste Biomass Valor. **13**, 2735–2747 (2022).
10. I. Istadi and Y. Bindar, Appl. Therm. Eng. **73**, 1129–1140 (2014).
11. S. Wang, X. Guo, K. Wang, and Z. Luo, J. Anal. Appl. Pyrolysis **91**, 183–189 (2011).
12. Y. Ramli, S. Steven, E. Restiawaty, and Y. Bindar, Bioenerg. Res. **15**, 1918–1926 (2022).
13. O. Ismail, M. Urbanus, H. Murage, and O. Francis, Int. J. Sci. Res. **5**, 1264–1268 (2016).
14. E. Restiawaty, Y. Bindar, K. Syukri, O. Syahroni, S. Steven, R. A. Pramudita, and Y. W. Budhi, Biomass Conv. Bioref. (2022).
15. P. Hernowo, S. Steven, E. Restiawaty, and Y. Bindar, J. Taiwan Inst. Chem. Eng. **139**, 104520 (2022).
16. A. Ganesh, P. D. Grover, and P. V. R. Lyer, Fuel **71**, 889 (1992).
17. S. Madusari, S. S. Jamari, N. I. A. A. Nordin, Y. Bindar, T. Prakoso, E. Restiawaty, and S. Steven, ChemBioEng Rev. **10**, 37–54 (2023).

18. P. Dockrill and F. Friedrich, “Increasing the Energy Efficiency of Boiler and Heater Installations”, in *Boilers and Heaters: Improving Energy Efficiency* (Natural Resources Canada, 2001), pp. 8–13.
19. B. Patro, Alexandria Eng. J. **55**, 193–202 (2016).
20. S. Ependi and T. B. Nur, IOP Conf. Ser:. Mater. Sci. Eng. **309**, 1–7 (2018).
21. A. M. Pantaleo, P. Ciliberti, S. Camporeale, and N. Shah, Energy Procedia **75**, 1609–1617 (2015).
22. S. Steven, E. Restiawaty, and Y. Bindar, Waste Biomass Valor. (2022).
23. B. Patel, Iran. J. Energy Environ. **3**, 123–128 (2012).
24. S. A. Parker and B. K. Walker, “Boilers and Fired Systems”, in *Energy Management Handbook, Eighth Edition* (2013), pp. 91–129.
25. D. K. Sarkar, “Fuels and combustion”, in *Thermal Power Plant Design and Operation*, edited by D. K. Sarkar, 1st ed. (Elsevier, 2015), pp. 91–137.
26. S. Steven, D. L. Friatnasary, A. K. Wardani, K. Khoiruddin, G. Suantika, and I. G. Wenten, IOP Conf. Ser.: Earth Environ. Sci. **963**, 012034 (2022).
27. O. Levenspiel, in *Chemical Reaction Engineering, Third Edition* (John Wiley & Sons, 1999), pp. 447–451.
28. F. I. Hai, K. Yamamoto, and C. H. Lee, *Membrane Biological Reactors: Theory, Modeling, Design, Management* (IWA Publishing, 2014).
29. W. McCabe, J. C. Smith, and P. Harriot, “Agitation and Mixing of Liquids”, in *Unit Operations of Chemical Engineering, 5th Edition* (McGraw Hill International, 1993), pp. 236, 264–265.
30. C. J. Geankoplis, “Agitation and Mixing of Fluids and Power Requirements”, in *Transport Processes and Unit Operations, Third Edition* (Prentice-Hall International, 1993), pp. 141–151.
31. S. Steven, E. Restiawaty, and Y. Bindar, J. Eng. Technol. Sci. **54**, 220304 (2022).
32. S. Steven, E. Restiawaty, and Y. Bindar, IOP Conf. Ser.: Earth Environ. Sci. **963**, 012050 (2022).
33. S. M. Walas, “Fluid Transfer Equipment”, in *Chemical Process Equipment Selection and Design*. (Butterworth-Hienemann, Oxford, 1990), pp. 129–168.
34. B. J. Ennis, W. Witt, R. Weinekötter, D. Sphar, E. Gommeran, R. H. Snow, T. Allen, G. J. Raymus, and J. D. Litster, “Solid-Solid Operations and Processing”, in *Perry’s Chemical Engineers’ Handbook, 8th Edition* (The McGraw-Hill Companies, Inc. 2008), p. 48.
35. C. J. Geankoplis, “Liquid-Liquid and Fluid-Solid Separation Processes”, in *Transport Processes and Unit Operations, Third Edition* (Prentice-Hall International, 1993), pp. 697–709.
36. L. Klemas and J. A. Bonila, *Packed Columns: Design and Performance* (Academic Press, 2000).
37. L. M. Branscomb, F. Kodama, and R. Florida, *Industrializing Knowledge: University-Industry Linkages in Japan and the United States* (The MIT Press, 1999).
38. I. G. Wenten, S. Steven, A. Dwiputra, Khoiruddin, and A. N. Hakim, J. Phys.: Conf. Ser. **877**, 012002 (2017).
39. P. G. Sasmita and I. G. Wenten, “Application of ultrafiltration in shrimp aquaculture: From lab to full-scale capacity”, in *Proceeding of International Congress on Membrane and Membrane Processes, Seoul Korea* (2005).
40. Y. Bindar, S. Steven, S. W. Kresno, P. Hernowo, E. Restiawaty, R. Purwadi, and T. Prakoso, Biomass Conv. Bioref. (2022).
41. T. Norton, D. W. Sun, J. Grant, R. Fallon, and V. Dodd, Bioresour. Technol. **98**, 2386–2414 (2007).
42. S. Steven, E. Restiawaty, P. Pasymi, I. M. Fajri, and Y. Bindar, Asia-Pac. J. Chem. Eng. **17**, e2805 (2022).
43. R. B. Bird, W. E. Stewart, and E. N. Lightfoot, *Transport Phenomena, Second Edition* (John Wiley & Sons, Inc., 2002).
44. C. J. Geankoplis, “Principles of Momentum Transfer and Applications”, in *Transport Processes and Unit Operations, Third Edition* (Prentice-Hall International, 1993), pp. 114–118.
45. ANSYS, *ANSYS Fluent Theory Guide 2019 R3* (ANSYS, Inc., 2019).
46. G. Lopez-Santana, A. Kennaugh, and A. Keshmiri, Fluids **7**, 1–20 (2022).
47. Y. N. Kim, C. Wu, and Y. Cheng, Chem. Eng. Sci. **66**, 5357–5365 (2011).
48. P. Pasymi, Y. W. Budhi, and Y. Bindar, ASEAN J. Chem. Eng. **20**, 88–98 (2020).
49. S. Steven, E. Restiawaty, P. Pasymi, and Y. Bindar, Braz. J. Chem. Eng. (2022).
50. P. Pasymi, Y. W. Budhi, and Y. Bindar, Jurnal Teknologi **82**, 91–100 (2020).
51. P. Pasymi, Y. W. Budhi, and Y. Bindar, J. Eng. Technol. Sci. **50**, 684–697 (2018).
52. P. Pasymi, Y. W. Budhi, and Y. Bindar, J. Phys.: Conf. Ser. **1090**, 1–8 (2018).
53. S. Steven, E. Restiawaty, P. Pasymi, and Y. Bindar, Powder Technol. **410**, 117883 (2022).
54. S. V. Patankar, *Numerical Heat Transfer and Fluid Flow* (New York, 1980).
55. T. J. Chung, *Computational Fluid Dynamics* (Cambridge, 2010).

56. Y. Bindar and A. Irawan, *Performance Evaluation of the Burners and Walking Beam Reheating Furnace*, (LAPI ITB, 2014).
57. K. Arnold and M. Stewart, "Three-Phase Oil and Water Separation", in *Surface Production Operations, Volume 1, Third Edition* (Gulf Professional Publishing, 2008), pp. 244–315.
58. I. Amri and Y. Bindar, "CFD Analysis on Sand Settling Behaviour n a Sand Removal Vessel from Produced Water of an Oil", in *Regional Conference on Chemical Engineering, Yogyakarta* (2014).
59. Y. Bindar and I. Amri, "Effect of an Additional Internal Baffle inside a Sand Removal Vessel on Sand Settling Efficiency", in *Regional Conference on Chemical Engineering, Yogyakarta* (2014).
60. Y. Bindar, *Computational Engineering on Multidimensional Turbulent Flows (Rekayasa Komputasi Aliran Turbulen Multidimensi)* (ITB Press, 2017).
61. S. A. Morsi and A. J. Alexander, J. Fluid Mech. **55**, 193–208 (1972).